Structure factor of model bidisperse ferrofluids with relatively weak interparticle interactions

Ekaterina Novak, Elena Minina, Elena Pyanzina, Sofia Kantorovich, and Alexey Ivanov

Citation: The Journal of Chemical Physics **139**, 224905 (2013); doi: 10.1063/1.4834635
View online: http://dx.doi.org/10.1063/1.4834635
View Table of Contents: http://scitation.aip.org/content/aip/journal/jcp/139/22?ver=pdfcov
Published by the AIP Publishing

Structure factor of model bidisperse ferrofluids with relatively weak interparticle interactions

Ekaterina Novak,[1] Elena Minina,[2] Elena Pyanzina,[1] Sofia Kantorovich,[1,3,a)] and Alexey Ivanov[1]

[1]*Institute of Mathematics, Department of Mathematical Physics, Ural Federal University, Lenin av. 51, 620000 Ekaterinburg, Russia*
[2]*Institute for Computational Physics, Universiät Stuttgart, Allmandring 3, 70569 Stuttgart, Germany*
[3]*Faculty of Physics, Computational Physics, University of Vienna, Sensengasse 8, 1090 Vienna, Austria*

(Received 27 August 2013; accepted 11 November 2013; published online 12 December 2013)

In the present manuscript we develop a theoretical approach to describe the pair correlation function of bidisperse magnetic dipolar hard- and soft-spheres. We choose bidisperse system as the first step to allow for polydispersity when studying thermodynamics of magnetic fluids. Using diagram technique we calculate the virial expansion of the pair correlation function up to the first order in density and fourth order in the dipolar strength. Even though, the radial distribution functions are extremely sensitive to the steric potential, we show that the behaviour of the isotropic centre-centre structure factor is almost indifferent to the type of the short-range repulsion. We extensively compare our theoretical results to the data of molecular dynamics simulations, which helps us to understand the range of validity of the virial expansion both on density and magnetic dipolar strength. We also investigate the influence of the granulometric composition on the height, width, and position of the structure factor first peak in order to clarify whether it is possible to extract structural information from experimentally measured small angle neutron scattering intensities. © *2013 AIP Publishing LLC*. [http://dx.doi.org/10.1063/1.4834635]

I. INTRODUCTION

Nowadays, soft magnetic materials with controllable macro-properties are gaining more-and-more applications in technology and medicine.[1–9] The majority of these applications relies on the microstructure of the material, which, in turn, is determined by the interparticle interactions inherent to the system under investigation. One of the examples of such a magnetic soft matter system is magnetic fluid, namely the stable suspension of magnetic single-domain nanoparticles in a nonmagnetic carrier.[10] For more than 30 years, the microstructure of ferrofluids has been thoroughly investigated in various experiments.[11–20] One of the mostly used and widely spread techniques to study the microstructure is by interpreting scattering patterns obtained via small angle neutron scattering (SANS).[21–27] These experiments result in the dependence of the so-called structure factor on the wave vector. Further, using inverse Fourier transform one obtains the pair correlation function (or the radial distribution function), which describes the average probability of finding a particle at a given distance from the other.[28] Even though it sounds straightforward, the interpretation of SANS results cannot be done without having a reliable theoretical model for both form factors of particles and clusters and the pair correlation functions. In other words, it is much more feasible to solve an inverse problem, i.e., employing a so-called bottom-up approach to calculate pair correlation functions on the basis of known Hamiltonians.

It turned out that the properties, such as scattering ones, magnetic response, thermal capacity, compressibility, etc., of magnetic fluids, namely of the suspensions of ferro- or ferrimagnetic nanoparticles in magneto-passive carriers, were strongly influenced by two factors: the magnetic dipole-dipole interaction between particles and particle polydispersity. In other words, any information extracted from aforementioned experimental findings is, first, very sensitive to even small experimental error-bars; second, it is crucially influenced by the model chosen for describing interparticle correlations.

Ferrofluid microstructure was extensively studied in computer experiments.[29–43] Many authors investigated structure factor and its relation to the microstructure of systems of dipolar hard- and soft-spheres. It was found that the structure factor being a collective property could indeed provide the knowledge about clusters or interparticle correlations, but alone, without any analytical model at hand, structure factor was not sufficient for unique interpretation of the microstructure.[44,45] Several analytical approaches have been proposed to this end and usually two distinct regimes are studied separately. In case of strong dipolar interactions, it is known that ferroparticles form chains.[18,29,32,41] For this regime, analytical approaches are based on the direct calculation of the radial distribution function on the basis of the cluster size distribution.[44,45] Whereas, if the dipole-dipole interaction is of the order of thermal energy, no clusters are formed, but the role of magnetic interparticle correlations turns out to be still prominent. To take these correlations into account one could use diagram expansion of the pair correlation function, which proved to be efficient for low ferroparticle densities.[46–49] Being rather successful, the aforementioned studies of low-interacting regime lack a serious feature, namely all known models for calculating structure

a)Electronic mail: sofia.kantorovich@univie.ac.at

factors of ferrofluids with magnetic dipole-dipole interaction of the order of thermal energy are monodisperse. However, polydispersity exerts a dramatic influence on the ferrofluid microstructure,[44,50] not to mention that all industrial magnetic liquids are inevitably polydisperse.

The aim of the present study is to develop a theoretical approach describing the pair correlation functions and structure factor for the systems of bidisperse hard- and soft-spheres. There were several theoretical studies dedicated to the thermodynamic properties of polydisperse hard-sphere mixtures.[51–55] Here, we would use these results as a reference point to construct the perturbation theory for dipole-dipole interaction. The choice of a bidisperse system is rather obvious: being, on the one hand, still rather simple, it appears to be the first step on the way to full polydispersity, on the other hand. Earlier it was found that the bidisperse approximation, if correctly chosen, provides a sufficient accuracy in describing thermodynamics of real polydisperse magnetic fluids.[50,56] Even though, the resulting analytical expressions calculated in this paper are rather long and cumbersome, they are useful for two main reasons: (i) this formalism allows to avoid running long series of computer simulations for various systems with different granulometric compositions (GCs) to construct an empiric pair correlation function for further usage; (ii) it makes it possible to describe separately the contributions of steric and dipolar interactions (in a real experiment that is simply impossible without a theoretical model at hand and in computer simulations it is computationally very costly).

This paper is organised as follows. First (Sec. II) we introduce the basic concept of diagram expansion, and show the general outline of the calculations (mathematical details can be found in the Appendix). As the next step (Sec. III) we introduce the systems under study and discuss the details of computer simulations. Section IV is divided into three parts. First (Subsection IV A), we provide an exhaustive analysis of pair correlation functions for hard- and soft-sphere repulsion, analysing the contributions of various diagrams and investigating the influence of the granulometric composition. Here we also study the behaviour of the structure factor. After comparing our theoretical predictions to the results of molecular dynamics computer simulations we discuss the range of validity of the developed theoretical approach in Subsection IV B. Having a valid theory at hand, we scrutinise the influence of the dipolar interactions, granulometric composition, and particle densities on the partial structure factors and structure factor peaks (Subsection IV C). The summary of the work and a short outlook are provided in the Conclusion.

Below we use the following abbreviations: structure factors will be addressed as SFs; pair correlation functions are shortened to PCF; similarly, radial distribution functions are denoted by RDFs; molecular dynamics simulations will be briefly denoted by MD simulations; finally, the letter *p* added to any of the previous abbreviations would mean "partial" and prefixes ss, sl, and ll abbreviate "small-small," "small-large," and "large-large" attributes of an observable.

II. THEORY: DIAGRAM EXPANSION

We aim at obtaining analytical expressions for the SFs and pSFs of a bidisperse mixture of dipolar hard- or soft-spheres. To this end, we start with calculation of PCFs for the latter systems in order to further Fourier-transform them.

According to the classical definition, a PCF can be represented as a series of volume fraction φ:[28]

$$g(r) = \sum_{k=2}^{\infty} \varphi^{k-2} B_k(r), \tag{1}$$

where B_k are analogues to virial coefficients and depend on the interparticle distance (r). In order to calculate them, it is necessary to fix the Hamiltonian of the system. In the present manuscript, we assume that the Hamiltonian contains only two interactions: the central steric short-range repulsion and non-central magnetic dipole-dipole interaction. As a steric pair potential (U_s) we will use either hard-sphere one:

$$U_{HS}(i,j) = \begin{cases} \infty & r_{ij} < d_{ij} \\ 0 & r_{ij} \geq d_{ij} \end{cases}, \tag{2}$$

or soft-sphere type, Weeks-Chandler-Andersen (WCA) potential:[57]

$$U_{WCA}(i,j) = \begin{cases} 4\varepsilon \left[\left(\frac{d_{ij}}{r_{ij}} \right)^{12} - \left(\frac{d_{ij}}{r_{ij}} \right)^{6} \right] + \varepsilon & r_{ij} < r_{ij}^{co} \\ 0 & r_{ij} \geq r_{ij}^{co} \end{cases}, \tag{3}$$

where $d_{i(j)}$ are particle $i(j)$ diameters, $d_{ij} = (d_i + d_j)/2$, $r_{ij}^{co} = 2^{1/6} d_{ij}$ is the value of the cutoff and the interparticle distance is characterised by the absolute value of the difference between particle i and j displacement vectors, $r_{ij} = |\mathbf{r}_{ij}| = |\mathbf{r}_i - \mathbf{r}_j|$. This potential is a repulsive part of the Lennard-Jones potential which is truncated at r_{ij}^{co} and shifted by the value of the depth of the potential wall ε.

Magnetic dipole-dipole interaction U_{dd} can be written as

$$U_{dd}(i,j) = \frac{\mu_0}{4\pi} \left[\frac{(\boldsymbol{\mu}_i \cdot \boldsymbol{\mu}_j)}{|\mathbf{r}_{ij}|^3} - 3 \frac{(\boldsymbol{\mu}_i \cdot \mathbf{r}_{ij})(\boldsymbol{\mu}_j \cdot \mathbf{r}_{ij})}{|\mathbf{r}_{ij}|^5} \right], \tag{4}$$

where $\boldsymbol{\mu}_{i(j)}$ are magnetic moments of particles $i(j)$ and μ_0 is the vacuum permeability. The intensity of the dipole-dipole interaction is determined by the characteristic parameter $\lambda_{ij} = \beta \mu_0 \mu_i \mu_j / 4\pi d_{ij}^3$ which shows the ratio of the magnetic interaction of two particles at the close contact with perfectly coaligned dipole moments to the thermal energy. Here and further, $\mu_i = |\boldsymbol{\mu}_i|$ is a magnitude of ith magnetic moment and β denotes the inverse thermal energy.

Introducing Mayer function $f(ij) = \exp[-\beta(U_{dd}(i,j) + U_s(i,j))] - 1$, the second and the third virial-type coefficients have the following form (with v being a characteristic volume):

$$B_2(r_{12}) = \langle f(12) + 1 \rangle_{12},$$

$$B_3(r_{12}) = \frac{1}{v} \int d\mathbf{r}_3 \langle [f(12)+1] f(23) f(13) \rangle_{123}$$

$$= \frac{1}{v} \int d\mathbf{r}_{13} \int d\mathbf{r}_{23} \langle (f(12)+1) f(13) f(23) \rangle_{\Omega_1,\Omega_2,\Omega_3}.$$

Here, $\langle .. \rangle_{12(123)}$ denotes the averaging over all magnetic moment orientations of particles 1, 2 (1, 2, 3). In the case of three

particles, one needs to also average over the displacement vectors $\mathbf{r}_{13}$ and $\mathbf{r}_{23}$:

$$\langle..\rangle_{123} = \frac{1}{16\pi^2}\int d\mathbf{r}_{13}\int d\mathbf{r}_{23}\int_0^{2\pi} d\omega_1\int_0^{\pi} d\zeta_1 \sin\zeta_1\int_0^{2\pi} d\omega_2 \times \int_0^{\pi} d\zeta_2 \sin\zeta_2\int_0^{2\pi} d\omega_3\int_0^{\pi} d\zeta_3 \sin\zeta_3(..),$$

where angles ω_i (polar angle) and ζ_i (azimuthal angle) determine the magnetic moment orientation of the ith dipolar particle in the spherical coordinate system.

Truncating the expression from Eq. (1) after B_3 we get the first-order density expansion of the RDF:

$$g(r_{12}) = B_2(r_{12}) + \varphi B_3(r_{12}). \tag{5}$$

Both B_2 and B_3 contain various averaging of the dipolar interaction. Using λ_{ij} as a parameter, one can expand the dipolar interaction in series:

$$\exp\left(-\beta U_{dd}(i,j)\right) = \sum_{n=0}^{\infty}\frac{\lambda_{ij}^n}{n!}\frac{d_{ij}^{3n}}{r^{3n}}[-\beta\hat{U}_{dd}(i,j)]^n, \tag{6}$$

where $[-\beta U_{dd}(i,j)]^n = \lambda_{ij}^n d_{ij}^{3n}[-\beta\hat{U}_{dd}(i,j)]^n/r^{3n}$, and $\hat{U}_{dd}(i,j)$ is the dipole-dipole interaction with unitary vectors. In the present paper we take into account all terms up to λ_{ij}^4.

A. Bidisperse system

Let us consider bidisperse system composed of two types of particles different in diameter: particles with smaller diameter d_s we will call small ones and bigger particles with diameter d_l will be addressed as large ones ($d_s < d_l$).

In the expansion given by Eqs. (5) and (6) each term can be associated with the diagram[28] in the vertices of which particles are located, and the diagram sides symbolise the type of the integral. We consider the set of two and three particle diagrams (see Fig. 1). In this figure, a single solid line represents $\exp[-\beta U_s(i,j)]$, double solid line is the Mayer function $f_s(ij) = \exp[-\beta U_s(i,j)] - 1$, and n dash lines are $[-\beta U_{dd}(i,j)]^n/n!$, $i,j \in \{s,l\}$. Importantly, only the diagrams I_{3c}, I_{3f}, and I_{3h} provide non-equal contributions when differently sized vertices 1 and 2 are mirrored. The integrals corresponding to each of the diagrams in Fig. 1 have the form

$$I_{2a} = \exp[-\beta U_s(1,2)], \tag{7}$$

$$I_{2b} = \exp[-\beta U_s(1,2)]\left\langle\frac{[-\beta U_{dd}(1,2)]^2}{2}\right\rangle_{12}, \tag{8}$$

$$I_{2c} = \exp[-\beta U_s(1,2)]\left\langle\frac{[-\beta U_{dd}(1,2)]^4}{4!}\right\rangle_{12}, \tag{9}$$

$$I_{3a} = \frac{1}{v}\exp[-\beta U_s(1,2)]\int d\mathbf{r}_3 f_s(23) f_s(13), \tag{10}$$

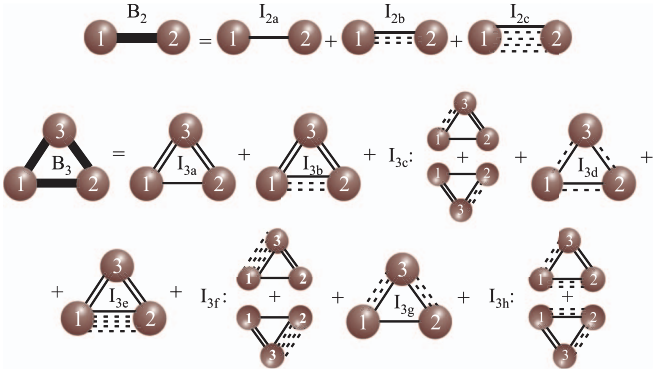

FIG. 1. Two particle and three particle diagrams which are taken into account for calculation of the pair correlation function for arbitrary sized particles (1,2,3). Note that only the diagrams I_{3c}, I_{3f}, and I_{3h} provide non-equal contributions when differently sized vertices 1 and 2 are mirrored. The functional forms of the integrals corresponding to lower subdiagrams for I_{3c}, I_{3f}, and I_{3h} are exactly the same as for the upper ones (provided below) and can be obtained by exchanging index 1 and index 2. A single solid line represents $\exp[-\beta U_s(i,j)]$, double solid line is the Mayer function $f_s(ij) = \exp[-\beta U_s(i,j)] - 1$, and n dash lines are $[-\beta U_{dd}(i,j)]^n/n!$, $i,j \in \{s,l\}$.

$$I_{3b} = \frac{1}{v}\exp[-\beta U_s(1,2)]\left\langle\frac{[-\beta U_{dd}(1,2)]^2}{2}\right\rangle_{12} \times \int d\mathbf{r}_3 f_s(23) f_s(13), \tag{11}$$

$$I_{3c} = \frac{1}{v}\exp[-\beta U_s(1,2)]\int d\mathbf{r}_3 f_s(23)\exp[-\beta U_s(1,3)] \times \left\langle\frac{[-\beta U_{dd}(1,3)]^2}{2}\right\rangle_{13}, \tag{12}$$

$$I_{3d} = \frac{1}{v}\exp[-\beta U_s(1,2)] \times \int d\mathbf{r}_3 \exp[-\beta U_s(1,3)]\exp[-\beta U_s(2,3)] \times \langle[-\beta U_{dd}(1,2)][-\beta U_{dd}(1,3)][-\beta U_{dd}(2,3)]\rangle_{123}, \tag{13}$$

$$I_{3e} = \frac{1}{v}\exp[-\beta U_s(1,2)]\left\langle\frac{[-\beta U_{dd}(1,2)]^4}{4!}\right\rangle_{12} \times \int d\mathbf{r}_3 f_s(23) f_s(13), \tag{14}$$

$$I_{3f} = \frac{1}{v}\exp[-\beta U_s(1,2)]\int d\mathbf{r}_3 f_s(23)\exp[-\beta U_s(1,3)] \times \left\langle\frac{[-\beta U_{dd}(1,3)]^4}{4!}\right\rangle_{13}, \tag{15}$$

$$I_{3g} = \frac{1}{v}\exp[-\beta U_s(1,2)] \times \int d\mathbf{r}_3 \exp[-\beta U_s(1,3)]\exp[-\beta U_s(2,3)] \times \left\langle\frac{[-\beta U_{dd}(1,3)]^2[-\beta U_{dd}(2,3)]^2}{4}\right\rangle_{123}, \tag{16}$$

$$I_{3h} = \frac{1}{v}\exp[-\beta U_s(1,2)] \times \int d\mathbf{r}_3 f_s(23)\exp[-\beta U_s(1,3)] \times \left\langle \frac{[-\beta U_{dd}(1,2)]^2[-\beta U_{dd}(1,3)]^2}{4} \right\rangle_{123}. \quad (17)$$

Since the system is bidisperse, the contribution of each diagram depends on the type of particles composing the diagram. If the steric repulsion was described by the hard-sphere potential, each diagram would depend only on the set of corresponding particle diameters, parameters λ_{ij}, and the distance between the 1st and the 2nd particle r. In case of the WCA potential, these diagrams would also depend on the energy parameter ε.

For the systems under study, one should consider separately PCFs for 3 possible particle pairs, namely to calculate pRDFs. The latter for large-large and small-small particle pairs would have the same functional form, whereas the "crossed" small-large PCF differs. Note that the symmetry of the system implies the equality between small-large and large-small pRDFs.

Let $v_{l(s)}$ be the volume of a large(small) particle, and $v_{sl} = (v_s^{1/3} + v_l^{1/3})^3/8$. The volume fractions of small and large particles are φ_s and φ_l, respectively. In two-particle diagrams no additional normalisation is needed, whereas for all three-particle diagrams the volume $v_{ij}(ii = i; jj = j)$ would be used as a characteristic normalisation volume. Using the notations introduced above, pPCFs can be presented in the following form:

- for large (ll) (small (ss)) particles

$$\begin{aligned} g_{ll(ss)}(r) = {} & I_{2a}(r, d_{l(s)}, d_{l(s)}) + I_{2b}(r, d_{l(s)}, d_{l(s)}, \lambda_{ll(ss)}) \\ & + I_{2c}(r, d_{l(s)}, d_{l(s)}, \lambda_{ll(ss)}) \\ & + \frac{\varphi_{l(s)}}{v_{l(s)}}[I_{3a}(r, d_{l(s)}, d_{l(s)}, d_{l(s)}) + I_{3b}(r, d_{l(s)}, d_{l(s)}, d_{l(s)}, \lambda_{ll(ss)}) \\ & + 2I_{3c}(r, d_{l(s)}, d_{l(s)}, d_{l(s)}, \lambda_{ll(ss)}) + I_{3d}(r, d_{l(s)}, d_{l(s)}, d_{l(s)}, \lambda_{ll(ss)}) \\ & + I_{3e}(r, d_{l(s)}, d_{l(s)}, d_{l(s)}, \lambda_{ll(ss)}) + 2I_{3f}(r, d_{l(s)}, d_{l(s)}, d_{l(s)}, \lambda_{ll(ss)}) \\ & + I_{3g}(r, d_{l(s)}, d_{l(s)}, d_{l(s)}, \lambda_{ll(ss)}) + 2I_{3h}(r, d_{l(s)}, d_{l(s)}, d_{l(s)}, \lambda_{ll(ss)})] \\ & + \frac{\varphi_{s(l)}}{v_{sl}}[I_{3a}(r, d_{l(s)}, d_{l(s)}, d_{s(l)}) + I_{3b}(r, d_{l(s)}, d_{l(s)}, d_{s(l)}, \lambda_{ll(ss)}) \\ & + 2I_{3c}(r, d_{l(s)}, d_{l(s)}, d_{s(l)}, \lambda_{sl}) + I_{3d}(r, d_{l(s)}, d_{l(s)}, d_{s(l)}, \lambda_{ll(ss)}, \lambda_{sl}) \\ & + I_{3e}(r, d_{l(s)}, d_{l(s)}, d_{s(l)}, \lambda_{ll(ss)}) + 2I_{3f}(r, d_{l(s)}, d_{l(s)}, d_{s(l)}, \lambda_{sl}) \\ & + I_{3g}(r, d_{l(s)}, d_{l(s)}, d_{s(l)}, \lambda_{sl}) + 2I_{3h}(r, d_{l(s)}, d_{l(s)}, d_{s(l)}, \lambda_{ll(ss)}, \lambda_{sl})]; \end{aligned} \quad (18)$$

- for small-large (sl) particles

$$\begin{aligned} g_{sl}(r) = {} & I_{2a}(r, d_s, d_l) + I_{2b}(r, d_s, d_l, \lambda_{sl}) + I_{2c}(r, d_s, d_l, \lambda_{sl}) \\ & + \frac{\varphi_s}{v_s}[I_{3a}(r, d_s, d_l, d_s) + I_{3b}(r, d_s, d_l, d_s, \lambda_{sl}) + I_{3c}(r, d_s, d_l, d_s, \lambda_{ss}) \\ & + I_{3d}(r, d_s, d_l, d_s, \lambda_{ss}, \lambda_{sl}) + I_{3e}(r, d_s, d_l, d_s, \lambda_{sl}) \\ & + I_{3f}(r, d_s, d_l, d_s, \lambda_{ss}) + I_{3g}(r, d_s, d_l, d_s, \lambda_{ss}, \lambda_{sl}) \\ & + I_{3h}(r, d_s, d_l, d_s, \lambda_{ss}, \lambda_{sl})] \\ & + \frac{\varphi_s}{v_{sl}}[I_{3c}(r, d_l, d_s, d_s, \lambda_{sl}) + I_{3f}(r, d_l, d_s, d_s, \lambda_{sl}) \\ & + I_{3h}(r, d_l, d_s, d_s, \lambda_{sl})] \\ & + \frac{\varphi_l}{v_{sl}}[I_{3a}(r, d_s, d_l, d_l) + I_{3b}(r, d_s, d_l, d_l, \lambda_{sl}) + I_{3c}(r, d_s, d_l, d_l, \lambda_{sl}) \\ & + I_{3d}(r, d_s, d_l, d_l, \lambda_{sl}, \lambda_{ll}) + I_{3e}(r, d_s, d_l, d_l, \lambda_{sl}) \\ & + I_{3f}(r, d_s, d_l, d_l, \lambda_{sl}) + I_{3g}(r, d_s, d_l, d_l, \lambda_{ll}, \lambda_{sl}) \\ & + I_{3h}(r, d_s, d_l, d_l, \lambda_{sl})] \\ & + \frac{\varphi_l}{v_l}[I_{3c}(r, d_l, d_s, d_l, \lambda_{ll}) + I_{3f}(r, d_l, d_s, d_l, \lambda_{ll}) + I_{3h}(r, d_l, d_s, d_l, \lambda_{ll}, \lambda_{sl})]. \end{aligned} \quad (19)$$

In the ss- and ll-pRDFs, the contributions of mirrored subdiagrams of I_{3c}, I_{3f}, and I_{3h} are equal, that is why one sees the prefactor 2. For the crossed terms, though, all contributions from mirrored subdiagrams are different, and as such are explicitly taken into account.

For dipolar hard-sphere system these pPCFs can be obtained analytically, as the calculation of all integrals (7)–(17) is possible. The analytical expressions are provided in the Appendix. For dipolar soft-sphere systems, however, the integrals (7)–(17) could be only partially simplified symbolically (dipolar contribution could be calculated analytically). The remaining averaging in the case of soft spheres we perform numerically. Note that also in case of dipolar soft spheres, the averaging is carried out in such a way that the parameters λ_{ij} remain prefactors, and the only dependence on the particle sizes, which enters the integrals, is the one through particle diameters d_i and not throughout the values of $|\mu_i|$. As a result, pPCFs in the case of dipolar soft-spheres will retain the same functional form as for a bidisperse hard-sphere system (18)–(19).

In order to calculate a centre-centre structure factor one needs to Fourier-transform the PCFs. Thus, taking into account that the system under study is invariant with respect to rotations, SFs depend on the modulus of the wave vector $|\mathbf{q}| = q$ and have the form

$$S_{ll(ss)}(q) = 1 + \frac{24\varphi_{l(s)}}{q d_{l(s)}^3} \int_0^\infty dr r \sin(qr) \left(g_{ll(ss)}(r) - 1\right), \tag{20}$$

$$S_{sl}(q) = 1 + \frac{24}{q} \left(\frac{\varphi_l}{d_l^3} + \frac{\varphi_s}{d_s^3}\right) \int_0^\infty dr r \sin(qr) \left(g_{sl}(r) - 1\right).$$

Here, the sum of the large particle volume fraction and small particle one is $\varphi_l + \varphi_s = \varphi$ and r stands for the interparticle distance (note that both q and r are scalars).

The total structure factor can be calculated analytically as a weighted superposition of the partial ones:

$$\begin{aligned} S_T(q) = {} & n_s \left\{1 + n_s \left(\frac{\varphi_l}{d_l^3} + \frac{\varphi_s}{d_s^3}\right) \frac{d_s^3}{\varphi_s} \left(S_{ss}(q) - 1\right)\right\} \\ & + n_l \left\{1 + n_l \left(\frac{\varphi_s}{d_s^3} + \frac{\varphi_l}{d_l^3}\right) \frac{d_l^3}{\varphi_l} \left(S_{ll}(q) - 1\right)\right\} \\ & + 2 n_s n_l \left(S_{sl}(q) - 1\right), \end{aligned} \tag{21}$$

where $n_s = \varphi_s/(\varphi_s + \varphi_l[d_s/d_l]^3)$ is the portion of small particles in the system and the portion of large ones is $n_l = 1 - n_s$.

In order to verify our theoretical approach we scrutinise two different bidisperse systems employing also molecular dynamics computer simulation.

III. SIMULATION DETAILS AND SYSTEM PARAMETERS

We performed MD simulations in ESPResSo,[58] using the simulation box with the volume fixed to $V = L^3$, where the length of the cubic box side was calculated as $L = 300/d_s$. We applied metallic periodic boundary conditions in all three directions and used standard Langevin thermostat, the description of which might be found in one of our previous works[44] for instance. In order to simulate long-range magnetic dipole-dipole interaction, we used dipolar-P3M.[59] Short range repulsion was modelled by the WCA potential (3). All lengths in the simulations were measured in d_s, thus the dimensionless diameter of the small particle was $\sigma_s = 1$; the diameter of the large particle in simulations was calculated as $\sigma_l = d_l/d_s$, in this case WCA cutoff radii were $r_{i,j}^{co} = 2^{-5/6}(\sigma_i + \sigma_j)$, $(i, j \in \{s, l\})$. The dimensionless temperature T^* as well as the energy parameter ε of the WCA potential were set to unity, that is why the values of the dimensionless particle dipole moments $\mu_{i(j)}^*$ could be calculated from λ_{ij}, in the following way: $\mu_s^* = \sqrt{\lambda_{ss}}$ and $\mu_l^* = \sqrt{\lambda_{ll}\sigma_l^3}$. The total number of particles in the simulation box was obtained as the sum of the number of large and small particles $N = N_l + N_s$, with $N_l = [\varphi_l V/v_l^*]$, $N_l = [\varphi_s V/v_s^*]$. Here, φ_i, $i \in \{s, l\}$ is the volume fraction of corresponding particles, $[\ \cdot\ ]$ denotes the integer part of the number in the square brackets, and $v_i^* = \sigma_i^3\pi/6$. Note that for every system, density, and granulometric composition, the number of particles was different.

TABLE I. Diameters and dipolar coupling constants of two bidisperse systems investigated here.

Name	d_s, nm (σ_s)	d_l, nm (σ_l)	λ_{ss}	λ_{ll}	λ_{sl}
S1	7.6 (1)	10.5 (1.38)	0.69	1.81	1.1
S2	13 (1)	17 (1.31)	0.69	2.34	1.24

For the theoretical model presented above, besides particle volume fractions and granulometric compositions of the samples, the strength of the magnetic dipole-dipole interaction plays an important part. To make the analysis broader we decided to consider two different bidisperse models (S1 and S2), whose parameters are presented in Table I.

In system S1 even the large particles are interacting rather weakly with each other, that is why we expect the results to be comparable to those for soft-sphere systems. Such a system would help us to pinpoint how important are the contributions of various diagrams. In system S2, on the other hand, the interaction between large particles is relatively strong, and actually seems to be compatible with the initial part of the chain-forming regime.[43] However, earlier studies of chain-forming bidisperse ferrofluids showed that the presence of small particles inhibit the growth of aggregates.[50] To this aim, for both systems, we would vary not only the total volume fraction φ, but also φ_l and φ_s, i.e., we would study various GCs. The volume fraction variations are summarised in Table II.

TABLE II. Total and partial volume fractions.

Total φ	GC1 φ_s, φ_l	GC2 φ_s, φ_l	GC3 φ_s, φ_l
0.05	0.02, 0.03	0.25, 0.25	0.03, 0.02
0.07	0.02, 0.05	0.35, 0.35	0.05, 0.02
0.09	0.02, 0.07	0.45, 0.45	0.07, 0.02
0.11	0.02, 0.09	0.55, 0.55	0.09, 0.02
0.13	0.02, 0.11	0.65, 0.65	0.11, 0.02

In this way, we go from the system in which the majority of particles is large, to the one with the small particles as a dominant fraction. Note that real ferrofluids usually contain a lot of small particles and only few large ones.[14,60,61] The total volume fraction changes in a wide range, which allows verifying the range of validity of the virial expansion performed above.

In simulations we calculated pRDFs (i.e., the normalised probability of finding a particle of a certain type at the given distance from the chosen one). Besides that, we directly computed the SFs, using the fact that in the absence of an external magnetic field the system remained invariant with respect to all possible rotations, and averaging over all wave vectors of magnitude $q = |\mathbf{q}|$ was sufficient to characterise the systems under study. Both pSFs and total SFs were calculated as in our previous studies:[44,47]

$$S(\mathbf{q}) = \frac{1}{N}\left\langle \left(\sum_{i=1}^{N} \sin \mathbf{q}\cdot\mathbf{r}_i\right)^2 + \left(\sum_{j=1}^{N} \cos \mathbf{q}\cdot\mathbf{r}_j\right)^2 \right\rangle, \quad (22)$$

where $\mathbf{r}_i$ and $\mathbf{r}_j$ are the position vectors of particles i and j, and N is the number of particles present in the system. In bidisperse systems, the structure factors for only large (small) particles are computed by disregarding in the sums over i and j the small (large) particles. It should be underlined that the values of the wave vectors $\mathbf{q}$ have to be compatible with the periodic boundary conditions, i.e., $\mathbf{q} \equiv (\mathbf{q_x}, \mathbf{q_y}, \mathbf{q_z}) = (2\pi/L)(l, m, n) \neq (0, 0, 0)$, where l, m, and n are integers.

Statistical error, in the following, is always smaller than the size of the symbols, representing simulation data. In terms of numbers, to reach this size of error-bars, first, 125×10^3 integrations were made in order to equilibrate the systems; the production run lasted another 75×10^6 integrations, while statistics was taken 25×10^3 steps; the reduced time-step was $\tau = 0.01$.

IV. RESULTS AND DISCUSSIONS

A. Different steric potentials

In this subsection we discuss the differences in pair correlation functions and structure factors induced by changing the steric part of the potential.

1. Pair correlations

In Fig. 2, we plot pair correlation functions for two different systems (S1 and S2, Table I) and all three granulometric compositions (Table II) with the total volume fraction fixed ($\varphi = 0.07$). In this figure three different types of pRDFs are presented: pRDFs calculated analytically for hard-sphere (see Eq. (2)) dipolar particles, those calculated in theory for dipolar soft-sphere systems (see Eq. (3)), and finally pRDFs obtained from MD simulations described above (Sec. III). Independently from the granulometric composition and values of dipolar coupling parameters λ_{ij}, pRDFs coincide for both potentials on the right from the first maximum. For any combination of (φ_s, φ_l), the pRDFs, calculated for the hard-sphere potential, strongly overestimate the height of the first peak. As for the pRDFs calculated for the soft-sphere steric potential, they show very good agreement with the simulation data. Note that the qualitative behaviour of the pRDF first peaks depending on the granulometric composition is not influenced by the type of steric interaction. Namely, the peak of the g_{sl} is always lower than the one of the g_{ll} and higher than that for g_{ss}. For dipolar hard-sphere system, one can always shift the position of the pRDFs first maximum by using an effective diameter (see, for example, Refs. 49 and 62) instead of the one for hard-spheres. However, in this case, the height of the peak remains almost the same. Besides that, the usage of an effective diameter removes the agreement between hard-sphere pRDFs and simulation data for higher interparticle distances

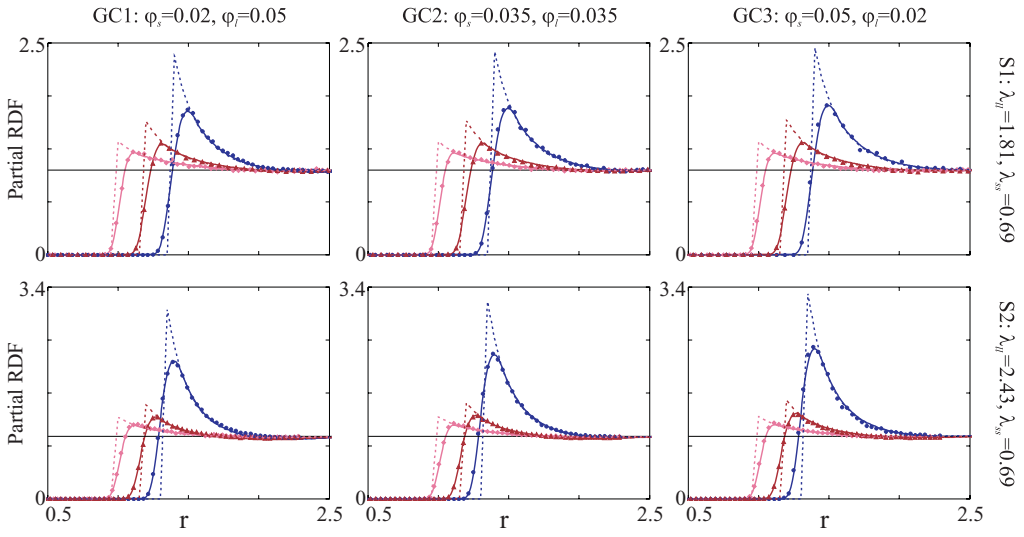

FIG. 2. Partial radial distribution functions for different bidisperse systems. Symbols correspond to the simulation data, solid lines describe the pRDFs obtained theoretically using the soft-sphere potential (3); dashed lines are theoretical predictions, in which hard-sphere potential (2) is considered. We use pink colour for g_{ss}, blue colour for g_{ll}, and brown colour for g_{sl} (both theory and computer simulations). The two rows correspond to two bidisperse systems (Table I): the first row is S1 ($\lambda_{ll} = 1.81$, $\lambda_{ss} = 0.69$) and the second one is S2 ($\lambda_{ll} = 2.34$, $\lambda_{ss} = 0.69$). Each column corresponds to different granulometric compositions (Table II): from the left to the right GC1 ($\varphi_s = 0.02$, $\varphi_l = 0.05$), GC2 ($\varphi_s = 0.035$, $\varphi_l = 0.035$), and GC3 ($\varphi_s = 0.05$, $\varphi_l = 0.02$). The total volume fraction is fixed, $\varphi = 0.07$.

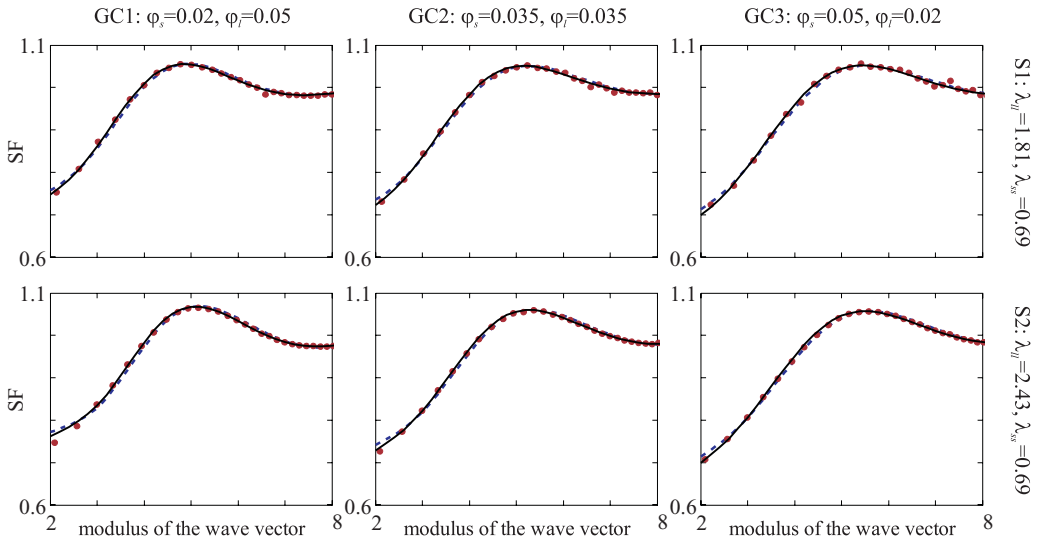

FIG. 3. Total structure factor *versus* the modulus of the wave vector q. Symbols correspond to the simulation data, black solid lines describe the SFs obtained theoretically using the soft-sphere potential (3); blue dashed lines are theoretical predictions, in which hard-sphere potential (2) is considered. The two rows correspond to two bidisperse systems (Table I): the first row is S1 ($\lambda_{ll} = 1.81$, $\lambda_{ss} = 0.69$) and the second one is S2 ($\lambda_{ll} = 2.34$, $\lambda_{ss} = 0.69$). Each column corresponds to different granulometric compositions (Table II): from the left to the right GC1 ($\varphi_s = 0.02$, $\varphi_l = 0.05$), GC2 ($\varphi_s = 0.035$, $\varphi_l = 0.035$), and GC3 ($\varphi_s = 0.05$, $\varphi_l = 0.02$). The total volume fraction is fixed, $\varphi = 0.07$.

(on the right from the first maximum), and in this way also makes the agreement between simulation and analytical SFs worse.

2. SFs

In fact, looking at Fig. 3, one sees that the discrepancies observed for dipolar hard-spheres in the pRDFs are vanishing when plotting the total structure factors. Here, we plot two analytical total SFs for systems S1 and S2 (Table I) for various granulometric compositions and compare them to the results of MD simulations. Good agreement could be found for a wide range of wave vectors.

The main conclusion from Figs. 2 and 3 is the following: when interpreting structure factor curves for various magnetic fluids and trying to extract PCFs, one needs to have an additional information about the type of short range interactions in the system.

Looking closer at the region of low-q, however, one sees that the diagram expansion fails to describe simulation data independently from the type of the steric potential, which is related to the fact that the long-distance correlations demand for higher order expansion with respect to φ. The latter suggests to pinpoint the ranges of densities and dipolar strengths, which our theory remains valid for.

B. Range of validity

The range of validity of the theory developed in the present work should be checked against two parameters: λ_{ij} and φ, as we use the double expansion of the PCF.

First, we address φ-limitations. In Fig. 4, we plot pRDFs and SFs for two different total densities ($\varphi = 0.09$ and $\varphi = 0.11$). We also plot the results for both S1 and S2. In order to underline the sensitivity of the developed theoretical approach to the parameters of the system, we plot pRDFs and SFs for two drastically different granulometric compositions. One can see that for the total volume fraction of 9% the agreement between the theory and simulations both for SFs and pRDFs remains acceptable as long as the density of large particles is small (lower left part of Fig. 4). If you keep the total volume fraction fixed but look at the granulometric composition GC1 ($\varphi_s = 0.02$ and $\varphi_l = 0.07$), it is seen that the theory starts deviating from the simulation data for ll-pRDF for the system with stronger interaction (see the upper left part of Fig. 4, pRDFs for S2). Note that the deviations in structure factor are weaker and affect only the range of small wave vectors. These deviations grow with increasing density (upper right part of Fig. 4). Here, for both systems S1 and S2 theoretical predictions are not that accurate any more. As expected, theory works rather well in case of GC3 (see the lower right part of Fig. 4). A closer look, however, reveals a discrepancy in the ss-pRDFs, related to the lack of higher order φ-terms if the density of small particles exceeds approximately 7%. Importantly, the structure factor is not sensitive to this lack of higher order concentration terms, and the theory keeps being close to the simulation data.

As we have just shown, the validity range of the theory depends not only on the density of particles, but also on the granulometric composition and interaction strength in the system. The latter dependence can be scrutinised easily by considering various λ_{ij}-contributions. Below we will investigate three different ways to truncate the series in Eq. (6): up to λ_{ij}^2, λ_{ij}^3 and the highest order will be λ_{ij}^4. The following procedure was used when plotting Fig. 5. Knowing that for total densities below 8% simulation data and theory agree well for both pRDFs and SFs, we set as a target function fourth-order λ_{ij} expansion, and started comparing it to the second- and third-order ones, looking for deviations. For pRDF we

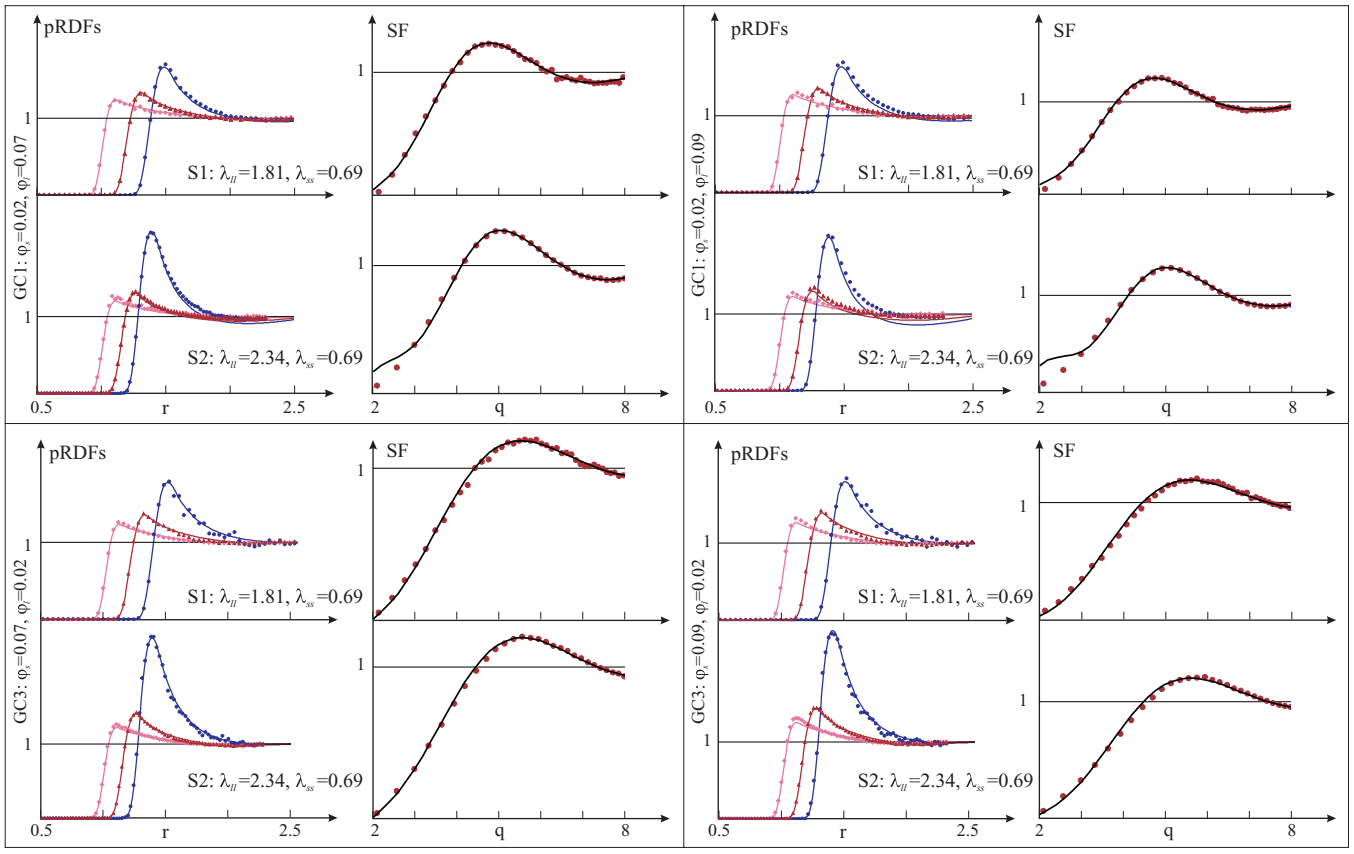

FIG. 4. pRDFs and SFs for two total volume fractions: $\varphi = 0.09$ (left side) and $\varphi = 0.11$ (right side). Symbols correspond to the simulation data, solid lines describe the results obtained theoretically using the soft-sphere potential (3). For RDFs the following colours are used: pink for g_{ss}, blue for g_{ll}, and brown for g_{sl} (both theory and computer simulations). The figure is divided into four rectangles. Each rectangle corresponds to a certain granulometric composition: in upper ones φ_s is fixed to 0.02, $\varphi_l = 0.07$ in the left rectangle and $\varphi_l = 0.09$ in the right one; in the lower rectangles φ_l is fixed to 0.02 and φ_s is correspondingly 0.07 (left) and 0.09 (right). Parameters are also provided in the body of the picture.

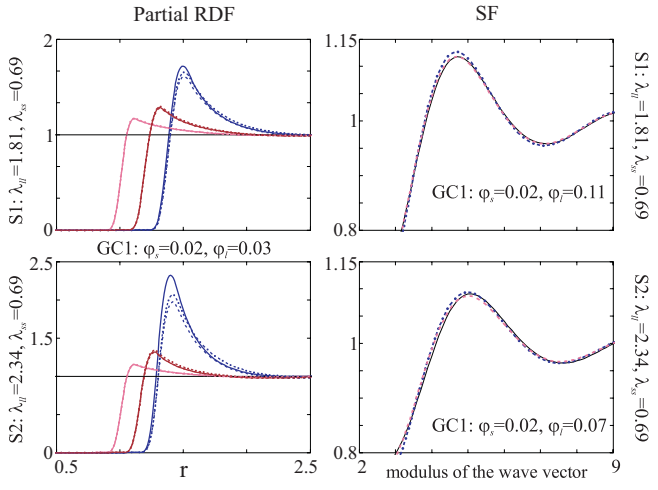

FIG. 5. Partial RDFs (left column) and SFs (right column) obtained theoretically using the soft-sphere potential (3). Solid lines describe the RDFs and SF obtained theoretically taking into account all terms up to λ_{ij}^4 in Eq. (6); dashed lines are theoretical predictions, in which all terms up to λ_{ij}^3 are considered, dashed-dotted lines are expansion up to λ_{ij}^2. For RDFs the following colours are used: pink for g_{ss}, blue for g_{ll}, and brown for g_{sl}. The two rows correspond to two bidisperse systems (Table I): the first row is S1 ($\lambda_{ll} = 1.81$, $\lambda_{ss} = 0.69$) and the second one is S2 ($\lambda_{ll} = 2.34$, $\lambda_{ss} = 0.69$). For RDFs we use granulometric composition GC1: $\varphi_s = 0.02$, $\varphi_l = 0.03$ (Table II); for SF two figures correspond to different granulometric compositions GC1: $\varphi_s = 0.02$, $\varphi_l = 0.11$ for top figure and $\varphi_s = 0.02$, $\varphi_l = 0.07$ for bottom one.

discovered them immediately: even for the lowest total density (0.05) ll-pRDFs calculated considering only λ_{ij}^2 terms differ significantly from those with λ_{ij}^3 and λ_{ij}^4 (see the left part of Fig. 5). Note that for ss-pRDFs the contributions from λ_{ij}^3 and λ_{ij}^4 are negligible, and any deviations observed for these pRDFs could only stem from the insufficiency in density terms. As for the sl-pRDFs, for the lowest density one can see only slight deviation of the λ_{ij}^2 expansion from λ_{ij}^3 one (λ_{ij}^4, here, is indistinguishable), but it grows with both density and λ_{ij}. Importantly, the deviations in structure factors appear for only higher densities and for the systems with dominant portions of large particles ($\varphi = 0.09$ for S2 and $\varphi = 0.11$ for S1, in both cases for the composition GC1, right part of Fig. 5). One can see that the difference between λ_{ij}-expansions is really small for SFs.

To summarise this part we would like to underline the following: experimentally measured structure factor can be well fitted with a simple λ_{ij}^2-approximation, using analytical hard-sphere diagrams. It is possible due to the fact of SFs being not sensitive enough to neither steric potential choice nor the order of dipolar potential λ_{ij}-expansion. This fitting will provide a set of three parameters: φ_s or φ_l, λ_{ss}, and λ_{ll}. With these parameters at hand, one can obtain pRDFs. To do that, however, one needs to use λ_{ij}^4-expansion and the adequate steric potential, as pRDFs are extremely sensitive to both choices.

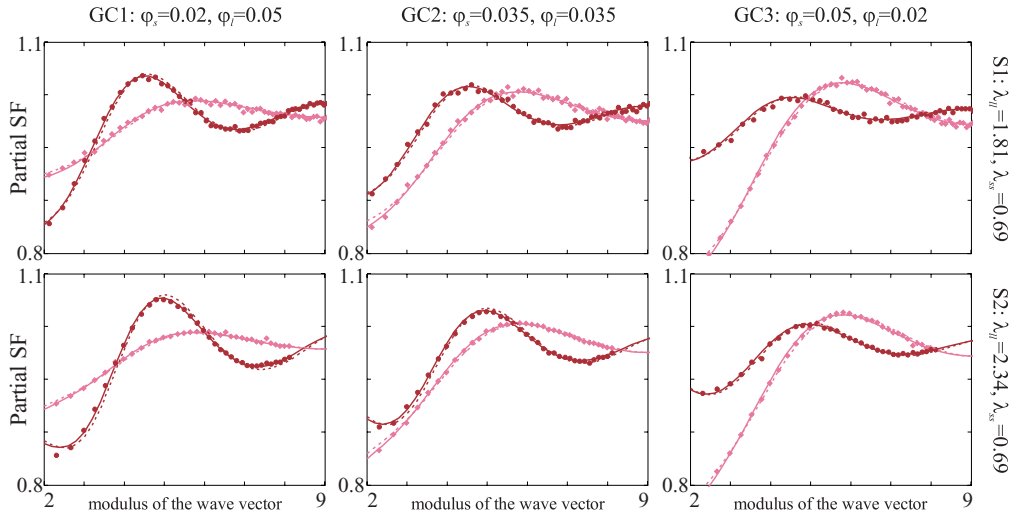

FIG. 6. Partial SFs *versus* the modulus of the wave vector. Symbols correspond to the simulation data, solid lines describe the pSFs obtained theoretically using the soft-sphere potential (3); dashed lines are theoretical predictions, in which hard-sphere potential (2) is considered. We use pink colour for S_{ss} and brown colour for S_{ll} (both theory and computer simulations). The two rows correspond to two bidisperse systems (Table I): the first row is S1 ($\lambda_{ll} = 1.81$, $\lambda_{ss} = 0.69$) and the second one is S2 ($\lambda_{ll} = 2.34$, $\lambda_{ss} = 0.69$). Each column corresponds to different granulometric compositions (Table II): from the left to the right GC1 ($\varphi_s = 0.02$, $\varphi_l = 0.05$), GC2 ($\varphi_s = 0.035$, $\varphi_l = 0.035$), and GC3 ($\varphi_s = 0.05$, $\varphi_l = 0.02$). The total volume fraction is fixed, $\varphi = 0.07$.

C. Characteristics of structure factors

In this section we show how granulometric composition and dipolar interaction strength could influence the behaviour of the structure factor first peak. We focus on the densities below 10%, so that theory and simulations agree well for both systems S1 and S2 with any GC.

1. pSFs

First, we plot pSFs in Fig. 6. Here, one can see that the agreement between simulation data and theory remains very good. For these plots one can see a difference between pSFs obtained for hard- and soft-spheres, albeit very small. We do not plot sl-pSFs here to avoid overloading the figures.

Partial SFs show a clear tendency: with growing small particle density the height of the ss-pSF increases and the width of the ss-pSF decreases (from the left to the right). Here, the total volume fraction of particles is fixed, thus, ll-pSF exhibits qualitatively the same behaviour with increasing φ_l (from the right to the left). To quantify the behaviour of the pSFs' first peaks we plot their heights and widths *versus* the volume fraction of small particles in Fig. 7. One can see that there is no big difference in the structure factor first peak height and width behaviour for systems S1 and S2, albeit for sl-pSF, for which width grows slightly for the system S2 and remains constant for S1. An important difference brought by the dipole-dipole interaction strength is the following: for small values of φ_s, the sl-pSF first peak is lower than that of ll-pSF, the range of densities for which this inequality holds true grows with growing λ_{ll} (check the position of the brown dashed-dotted and blue dashed lines in the left part of Fig. 7). It is caused by the two competing effects. On the one hand, the number of small-large particle possible pairs grows with growing φ_s, on the other hand, two large particles are strongly correlated.

In order to understand how the differences in pSFs for various systems and granulometric compositions affect the total SF behaviour, we present the characteristics of the total SF first peak in colour diagrams (Fig. 8). These diagrams have the following structure: by choosing the granulometric composition (φ_s along the abscissa and φ_l along the ordinate), you can see which would be the position (leftmost column), the height (middle column), and the width of the total SF for system S1 (upper row) and system S2 (lower row). The diagrams show that the overall influence of dipole-dipole interaction strength

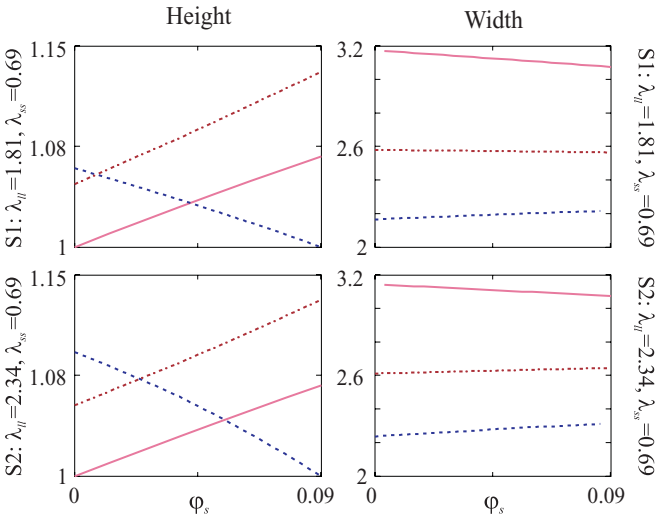

FIG. 7. Characteristics of the pSFs first peak. Pink solid lines describe theoretical predictions for S_{ss}; blue dashed lines are the theoretical prediction for S_{ll}; and curves corresponding to S_{sl} are plotted by brown dashed-dotted line. The two rows correspond to two bidisperse systems (Table I): the first row is S1 ($\lambda_{ll} = 1.81$, $\lambda_{ss} = 0.69$) and the second one is S2 ($\lambda_{ll} = 2.34$, $\lambda_{ss} = 0.69$). The left column contains the plots showing the height of the first peak as a function of φ_s; in the right column we present the width of the first peak as a function of φ_s. The total volume fraction is fixed, $\varphi = 0.09$. Simulation results being in a very good agreement (for this density) with our theory are not provided here for the sake of clarity.

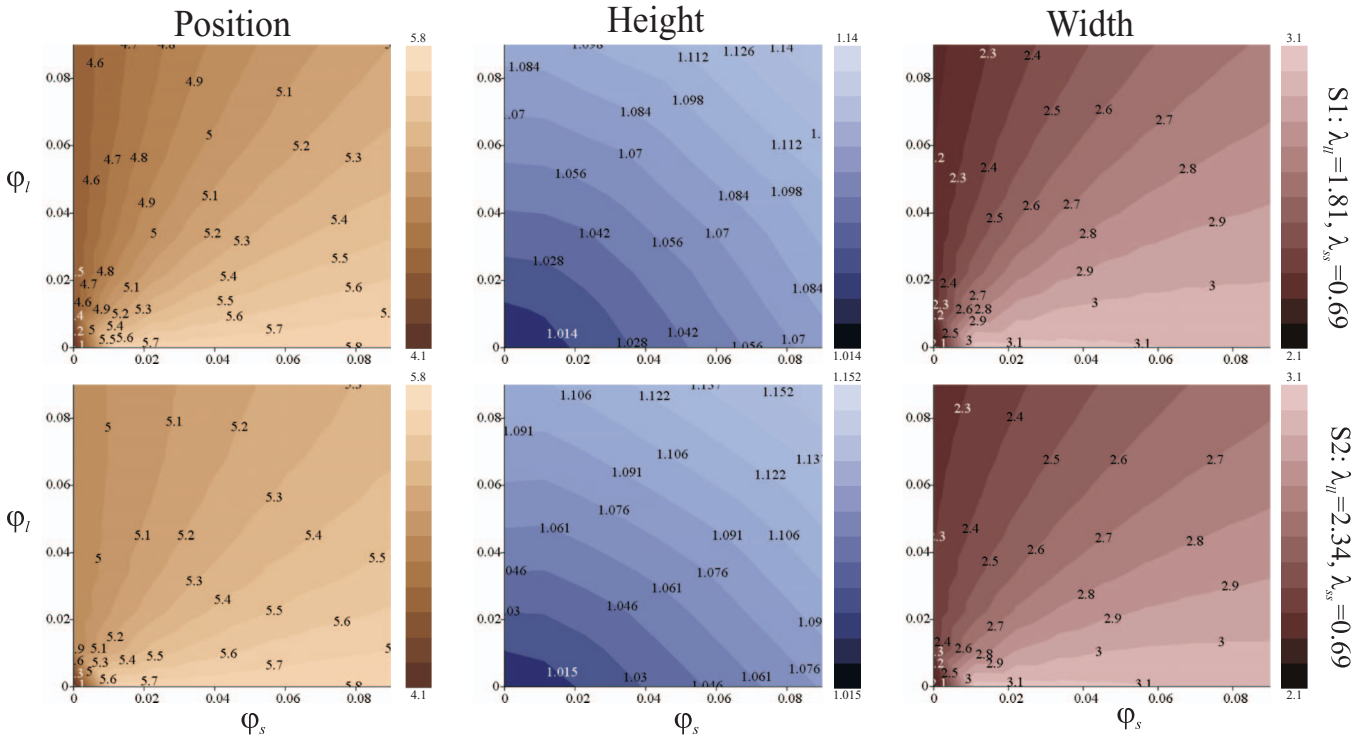

FIG. 8. φ_s–φ_l colour diagrams. The two rows correspond to two bidisperse systems (Table I): the first row is S1 ($\lambda_{ll} = 1.81$, $\lambda_{ss} = 0.69$) and the second one is S2 ($\lambda_{ll} = 2.34$, $\lambda_{ss} = 0.69$). In all diagrams we plot φ_s along the abscissa and φ_l along the ordinate. In the first column the numbers and the colours stay for the SF first peak position; the second column contains the information about the height of the SF first peak; in the third column the corresponding SF first peak width is presented.

is not big (compare numbers in two rows), whereas the granulometric composition influences all three observables rather strongly. The position of the SF first peak changes by 20% when going from a monodisperse large particle system to a monodisperse small particle system. That is due to the change of the most probable contact distance in these systems. The height of the SF first peak does not change much (within 10%), and exhibits the strongest increase along the bisector line of the diagram as it is directly correlated with the total number density of particles in the system. The width of the first peak grows with increasing density of small particles due to diminishing dipolar correlations which can hold particles on average closer to each other (up to 30% difference can be observed).

Thus, measuring these three characteristics of the SF first peak for different ferrofluids, one can extract at least qualitative information about the changes in the granulometric composition and interaction strengths in the system, analogously as it was shown before for non-dipolar self-assembling systems.[45]

V. CONCLUSION

In the present manuscript we developed a theoretical approach to calculate pair correlation functions for model bidisperse hard- and soft-spheres based on the virial expansion in the absence of an external magnetic field. From that, we calculated partial and total structure factors. We found that the steric potential does not play a crucial part in the qualitative behaviour of structure factors, however, when interpreting experimental results it is absolutely essential to know the short range part of the interactions, as the pair correlation functions are extremely sensitive to the latter. In other words, in order to predict the structure factor of a certain system one can use analytically available formulas for the pair correlation functions. Despite that, in order to get the information about the thermodynamics of the system on the basis of scattering patterns, one needs a model, where both steric and dipolar interactions are properly taken into account. Our theory was verified against the data of molecular dynamics simulations and proved to be in good agreement.

We analysed the influence of the granulometric composition on the SF first peak position, width, and height. To this end, we were able to develop a method of extracting the dominant fraction of particles from these three parameters.

The theory developed here is valid for the systems in which total volume fraction does not exceed 10%. It is due to the fact that the expansion of the pair correlation function is performed up to the three-particle diagrams, which for dense systems is not enough. One of the possible extensions of this approach might be to employ known pair correlations for the systems of pure hard-spheres.[63,64] Nonetheless, the majority of commercially used ferrocolloids are not that dense, and already the theory proposed here would be sufficient. As for the dipolar strength, there is no need to introduce higher order expansion with respect to the dipolar coupling constant: it is well-known that for λ_{ij} higher than $\sim$ 2–3 the chain formation takes place in the system. In this case, a different approach should be used to describe thermodynamic properties of the aggregate-forming soft- and hard-sphere dipolar systems.[44,45]

Note that the terms related to λ_{ij}^4 become important in the expansion, put forward here, only for the systems, in which either the portion of large particles is significant, or the dipolar interactions for the cross-correlations become pronounced.

In future, we would like to apply our theoretical model to calculate compressibility and osmotic pressure of model bidisperse systems of dipolar hard- and soft-spheres. Besides that, we would like to underline that all diagrams for dipolar hard-spheres were calculated in a general form, meaning that if more fractions are considered, the formulas obtained here can be used to analyse pair correlations of really "polydisperse" systems. To this end, we are currently investigating how strong is the contribution from polydispersity in comparison to a bidisperse approximation.

ACKNOWLEDGMENTS

The work was done in the framework of the Russian Federation for Basic Research (RFBR) Grant No. 12-02-12063-ofi-m. S.K. is grateful to RFBR Grant mol-a-ved 12-02-33106, and has been supported by Ministry of Science and Education of RF 2.609.2011 and by Austrian Science Fund (FWF): START-Projekt Y 627-N27. E.N. and E.P. were supported by RFBR Grant mol-a 12-02-31330.

APPENDIX: CALCULATIONS OF THE DIAGRAMS FOR HARD-SPHERE DIPOLAR PARTICLES

Here, we show how the diagrams were calculated, and provide all the resulting analytical expressions for a bidisperse system made of the dipolar hard spheres.

Calculations of the two-particle diagrams are straightforward and give the following compact result:

$$I_{2a}(r,d_1,d_2)+I_{2b}(r,d_1,d_2,\lambda_{12})+I_{2c}(r,d_1,d_2,\lambda_{12}) = \begin{cases} 0 & r<d_{12} \\ 1+\dfrac{\lambda_{12}^2}{3}\left(\dfrac{d_{12}}{r}\right)^6+\dfrac{\lambda_{12}^4}{25}\left(\dfrac{d_{12}}{r}\right)^{12} & r\geq d_{12} \end{cases}, \quad \text{(A1)}$$

where d_1, d_2 are the diameters of the first and the second particle, respectively, $d_{ij}=(d_i+d_j)/2$ ($i,j\in\{1,2\}$ for two-particle diagrams and $i,j\in\{1,2,3\}$ for the three-particle ones).

The contributions of three-particle diagrams to the pair correlation function are much more cumbersome. The main difficulty stems from the integration limits. When two particles of arbitrary size are fixed the third particle, depending on its size and on the distance between the first two, might either pass between particles 1 and 2 or might have a spatial constraint. It means that each integral in Eqs. (10)–(17) is split into three according to the distance between particles 1 and 2 and the size of the third (see Fig. 9). Limits of these cases are to be found solving a set of algebraic equations. Below we represent all diagram contributions for every case separately.

1. $r<d_{12}$

The first constraint is given by the fact that the particles 1 and 2 are hard spheres and, as a result, cannot penetrate into each other (see Fig. 9(a)). Thus, for such a distance $r<d_{12}$ the contribution to Eqs. (10)–(17) equals zero.

2. $d_{12}\leq r\leq d_{13}+d_{23}$

In this case the distance between particles 1 and 2 is not large enough for the third particle to pass between them, as it is shown in Fig. 9(b). This leads to the following contributions to Eqs. (10)–(17):

$$I_{3a}(r,d_1,d_2,d_3)=\frac{1}{2rd_{13}^3}\sum_{i=0}^{4} r^i f_i(d_{13},d_{23}), \quad \text{(A2)}$$

with the polynomial coefficients

$$f_0(d_{13},d_{23})=-3\left(d_{13}^2-d_{23}^2\right)^2,$$
$$f_1(d_{13},d_{23})=8\left(d_{13}^3+d_{23}^3\right),$$
$$f_2(d_{13},d_{23})=-6\left(d_{13}^2+d_{23}^2\right),$$
$$f_3(d_{13},d_{23})=0, \quad f_4(d_{13},d_{23})=1;$$

$$I_{3b}(r,d_1,d_2,d_3,\lambda_{12})=I_{3a}(r,d_1,d_2,d_3)\frac{\lambda_{12}^2}{3}\left(\frac{d_{12}}{r}\right)^6; \quad \text{(A3)}$$

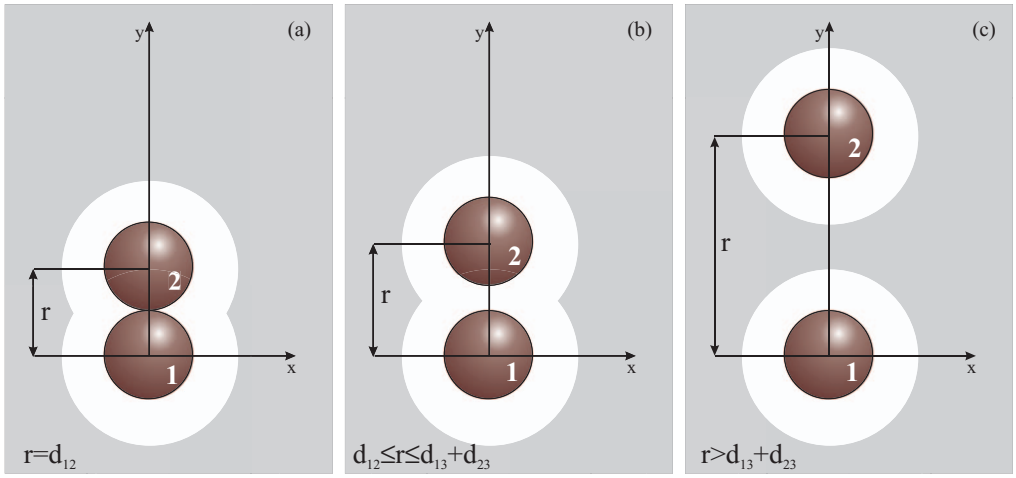

FIG. 9. Available area where the third particle can be located according to the distance between particles 1 and 2. This area is depicted in grey colour and the area in white is excluded area: (a) corresponds to a boundary case when the particles 1 and 2 are in close contact ($r=d_{12}$); (b) the third particle cannot pass between the particles 1 and 2 ($d_{12}\leq r\leq d_{13}+d_{23}$); (c) the distance between the centres of the particles 1 and 2 is large enough that the third particle can pass between them ($r>d_{13}+d_{23}$).

$$I_{3c}(r, d_1, d_2, d_3, \lambda_{13}) = \lambda_{13}^2 d_{13}^3 F_{3c}(d_{13}, r + d_{23}, r, d_{23}), \quad \text{(A4)}$$

where $F_{3c}(x, y)$ has the following form:

$$F_{3c}(x, y, r, d_{23}) = \frac{(r^2 - d_{23}^2)(y^4 - x^4)}{2rx^4y^4} - \frac{4}{3}\frac{y^3 - x^3}{x^3y^3} + \frac{y^2 - x^2}{rx^2y^2}; \quad \text{(A5)}$$

$$I_{3d}(r, d_1, d_2, d_3, \lambda_{12}, \lambda_{13}, \lambda_{23}) = \frac{\lambda_{12}\lambda_{13}\lambda_{23}d_{12}^3}{18r^6d_{13}^3}[r^2 - (d_{13} - d_{23})^2]^2 \times \left[r^2 - d_{13}^2 - 4d_{13}d_{23} - d_{23}^2\right]; \quad \text{(A6)}$$

$$I_{3e}(r, d_1, d_2, d_3, \lambda_{12}) = I_{3a}(r, d_1, d_2, d_3)\frac{\lambda_{12}^4}{25}\left(\frac{d_{12}}{r}\right)^{12}; \quad \text{(A7)}$$

$$I_{3f}(r, d_1, d_2, d_3, \lambda_{13}) = \frac{\lambda_{13}^4 d_{13}}{25(r + d_{23})^8}\left[\frac{3(r - d_{23})[(r + d_{23})^{10} - d_{13}^{10}]}{5rd_{13}^2(r + d_{23})} - \frac{4[(r + d_{23})^9 - d_{13}^9]}{3d_{13}(r + d_{23})} + \frac{3[(r + d_{23})^8 - d_{13}^8]}{4r}\right]; \quad \text{(A8)}$$

$$I_{3g}(r, d_1, d_2, d_3, \lambda_{13}, \lambda_{23}) = \lambda_{13}^2\lambda_{23}^2 d_{13}^3 d_{23}^6\left[\frac{49}{4r^9}\ln\left[\frac{d_{13}d_{23}}{(r + d_{13})(r + d_{23})}\right] + F_{3g}(r, d_{23}) + F_{3g}(r, d_{13}) + \frac{1}{720rd_{13}^6d_{23}^6}\sum_{i=0}^{4} r^i f_i(d_{13}, d_{23})\right], \quad \text{(A9)}$$

where the polynomial coefficients $f_i(d_{13}, d_{23})$ for $i = \overline{0, 4}$ have the following form:

$$f_0(d_{13}, d_{23}) = 6d_{13}^4 + 6d_{23}^4 + 63d_{13}^2d_{23}^2, \quad f_1(d_{13}, d_{23}) = 0,$$

$$f_2(d_{13}, d_{23}) = -6\left(d_{13}^2 + d_{23}^2\right), \quad f_3(d_{13}, d_{23}) = 0,$$

$$f_4(d_{13}, d_{23}) = 2,$$

and $F_{3g}(r, x)$ is given by (A10):

$$F_{3g}(r, x) = \frac{1}{720r^8x^6(r + x)^3}\sum_{i=0}^{8} r^i x^{8-i} g_i, \quad \text{(A10)}$$

with the following polynomial coefficients:

$$g_0 = 8820, \quad g_1 = 22\,050, \quad g_2 = 16\,170, \quad g_3 = 2205,$$

$$g_4 = -441,$$

$$g_5 = 147, \quad g_6 = -63, \quad g_7 = -6, \quad g_8 = -2;$$

$$I_{3h}(r, d_1, d_2, d_3, \lambda_{12}, \lambda_{13}) = \frac{\lambda_{12}^2\lambda_{13}^2 d_{12}^6}{r^9 d_{13}^3}\left[\frac{d_{13}^6}{60}\ln\left(\frac{r + d_{23}}{d_{13}}\right) + \frac{1}{720(r + d_{23})^3}\sum_{i=0}^{9} f_i(d_{13}, d_{23})r^i\right], \quad \text{(A11)}$$

where the polynomial coefficients $f_i(d_{13}, d_{23})$ are given by the following expressions:

$$f_0(d_{13}, d_{23}) = d_{23}^3\left(d_{13}^2 - d_{23}^2\right)\left(11d_{13}^4 - 7d_{13}^2d_{23}^2 + 2d_{23}^4\right),$$

$$f_1(d_{13}, d_{23}) = 3d_{23}^2\left(d_{13}^2 - 2d_{23}^2\right)\left(7d_{13}^4 - 4d_{13}^2d_{23}^2 + d_{23}^4\right),$$

$$f_2(d_{13}, d_{23}) = 3d_{13}^2d_{23}\left(60d_{13}^2d_{23}^2 - 37d_{13}^4 - 33d_{23}^4\right),$$

$$f_3(d_{13}, d_{23}) = 16d_{23}^6 - 369d_{13}^2d_{23}^4 - 320d_{13}^3d_{23}^3 + 684d_{13}^4d_{23}^2 - 33d_{13}^6,$$

$$f_4(d_{13}, d_{23}) = 3d_{23}\left(234d_{13}^4 - 320d_{13}^3d_{23} - 87d_{13}^2d_{23}^2 + 4d_{23}^4\right),$$

$$f_5(d_{13}, d_{23}) = 3\left(78d_{13}^4 - 320d_{13}^3d_{23} + 75d_{13}^2d_{23}^2 - 4d_{23}^4\right),$$

$$f_6(d_{13}, d_{23}) = 351d_{13}^2d_{23} - 320d_{13}^3 - 16d_{23}^3,$$

$$f_7(d_{13}, d_{23}) = 117d_{13}^2, \quad f_8(d_{13}, d_{23}) = 6d_{23},$$

$$f_9(d_{13}, d_{23}) = 2.$$

3. $r > d_{13} + d_{23}$

In this case the distance between the particles 1 and 2 is so large that the third particle can be located between them as it is shown in Fig. 9(c). This leads to the following contribution of diagrams:

$$I_{3a}(r, d_1, d_2, d_3) = I_{3b}(r, d_1, d_2, d_3, \lambda_{12}) = I_{3e}(r, d_1, d_2, d_3, \lambda_{12}) = 0; \quad \text{(A12)}$$

$$I_{3c}(r, d_1, d_2, d_3, \lambda_{13}) = \lambda_{13}^2 d_{13}^3 F_{3c}(r - d_{23}, r + d_{23}, r, d_{23}), \quad \text{(A13)}$$

where $F_{3c}(x, y)$ is given by (A5).

$$I_{3d}(r, d_1, d_2, d_3, \lambda_{12}, \lambda_{13}, \lambda_{23}) = -\frac{16\lambda_{12}\lambda_{13}\lambda_{23}d_{12}^3d_{23}^3}{9r^6}; \quad \text{(A14)}$$

$$I_{3f}(r, d_1, d_2, d_3, \lambda_{13}) = -\frac{24\lambda_{13}^4 d_{13}^9 d_{23}^3}{1125}\frac{15r^6 + 63r^4d_{23}^2 + 45r^2d_{23}^4 + 5d_{23}^6}{\left(r^2 - d_{23}^2\right)^9}; \quad \text{(A15)}$$

$$I_{3g}(r, d_1, d_2, d_3, \lambda_{13}, \lambda_{23}) = \lambda_{13}^2\lambda_{23}^2 d_{13}^3 d_{23}^6 \left[\frac{49}{4r^9} \ln \left[\frac{(r-d_{13})(r-d_{23})}{(r+d_{13})(r+d_{23})} \right] + G_{3g}(r, d_{13}) + G_{3g}(r, d_{23}) \right], \quad \text{(A16)}$$

where $G_{3g}(r, x)$ is given by

$$G_{3g}(r, x) = \frac{1}{90r^8x^3(x^2-r^2)^3} \sum_{i=0}^{8} g_i x^{8-i} r^i,$$

with the following polynomial coefficients:

$$g_0 = 2205, \quad g_1 = 0, \quad g_2 = -5880, \quad g_3 = 0,$$

$$g_4 = 4851, \quad g_5 = 0, \quad g_6 = -1008, \quad g_7 = 0, \quad g_8 = -80;$$

$$I_{3h}(r, d_1, d_2, d_3, \lambda_{12}, \lambda_{13}) = \frac{\lambda_{12}^2\lambda_{13}^2 d_{12}^6 d_{13}^3}{r^9} \left[\frac{1}{60} \ln \left(\frac{r+d_{23}}{r-d_{23}} \right) + \frac{r d_{23}\left(3r^4 + 88r^2 d_{23}^2 - 3d_{23}^4\right)}{90(d_{23}^2 - r^2)^3} \right]. \quad \text{(A17)}$$

In case of equal diameters these formulas coincide with those obtained for a monodisperse system of dipolar hard-spheres.[46]

[1] A. Lubbe, C. Alexiou, and C. Bergemann, "Clinical applications of magnetic drug targeting," J. Surg. Res. **95**, 200–206(7) (2001).
[2] J. Dobson, "Magnetic micro- and nano-particle-based targeting for drug and gene delivery," Nanomedicine **1**, 31–37 (2006).
[3] M. E. Hayden and U. O. Häfeli, "Magnetic bandages for targeted delivery of therapeutic agents," J. Phys.: Condens. Matter **18**, S2877 (2006).
[4] J. Durán, J. Arias, V. Gallardo, and A. Delgado, "Magnetic colloids as drug vehicles," J. Pharm. Sci. **97**, 2948–2983 (2008).
[5] S. Hughes, S. McBain, J. Dobson, and A. J. El Haj, "Selective activation of mechanosensitive ion channels using magnetic particles," J. R. Soc., Interface **5**, 855–863 (2008).
[6] Q. A. Pankhurst, N. T. K. Thanh, S. K. Jones, and J. Dobson, "Progress in applications of magnetic nanoparticles in biomedicine," J. Phys. D: Appl. Phys. **42**, 224001 (2009).
[7] C. S. Brazel, "Magnetothermally-responsive nanomaterials: Combining magnetic nanostructures and thermally-sensitive polymers for triggered drug release," Pharm. Res. **26**, 644–656 (2009).
[8] E. Pollert, G. Goglio, S. Mornet, and E. Duguet, "Magnetic nanoparticles for magnetic resonance imaging and hyperthermia applications," in *Nanomaterials: A Danger or a Promise?*, edited by R. Brayner, F. Fiévet, and T. Coradin (Springer London, 2013), pp. 99–129.
[9] D. Ortega, N. Perez, J. L. Vilas, J. S. Garitaonandia, K. Suzuki, J. R. Marin, and M. Rodriguez, "Nonylphenol polyethoxylate coated body-center-cubic iron nanocrystals for ferrofluids with technical applications," J. Appl. Phys. **113**, 17B505 (2013).
[10] L. Resler and R. E. Rosensweig, "Magnetocaloric power," AIAA J. **2**, 1418–1422 (1964).
[11] Y. N. Skibin, V. V. Chekanov, and Y. L. Raikher, "Birefringence in a ferromagnetic liquid," J. Exp. Theor. Phys. **45**, 496–499 (1977).
[12] P. C. Scholten, "The origin of magnetic birefringence and dichroism in magnetic fluids," IEEE Trans. Magn. **16**, 221–225 (1980).
[13] S. Taketomi, "Magnetic fluids anomalous pseudo-cotton mouton effects about 10^7 larger than that of nitrobenzene," Jpn. J. Appl. Phys. **22**, 1137–1143 (1983).
[14] V. Buzmakov and A. Pshenichnikov, "On the structure of microaggregates in magnetite colloids," J. Colloid Interface Sci. **182**, 63–70 (1996).
[15] S. Odenbach and H. Gilly, "Taylor vortex flow of magnetic fluids under the influence of an azimuthal magnetic field," J. Magn. Magn. Mater. **152**, 123 (1996).
[16] S. Odenbach, *Magnetoviscous Effects in Ferrofluids*, Lecture Notes in Physics Vol. 71 (Springer, Berlin, 2002).
[17] G. Meriguet, E. Dubois, A. Bourdon, G. Demouchy, V. Dupuis, and R. Perzynski, "Forced Rayleigh scattering experiments in concentrated magnetic fluids: effect of interparticle interactions on the diffusion coefficient," J. Magn. Magn. Mater **289**, 39 (2005).
[18] M. Klokkenburg, R. P. A. Dullens, W. K. Kegel, B. H. Erné, and A. P. Philipse, "Quantitative real-space analysis of self-assembled structures of magnetic dipolar colloids," Phys. Rev. Lett. **96**, 037203 (2006).
[19] B. Luigjes, D. M. E. Thies-Weesie, A. P. Philipse, and B. H. Erné, "Sedimentation equilibria of ferrofluids: I. Analytical centrifugation in ultrathin glass capillaries," J. Phys.: Condens. Matter **24**, 245103 (2012).
[20] B. Luigjes, D. M. E. Thies-Weesie, B. H. Ern, and A. P. Philipse, "Sedimentation equilibria of ferrofluids: II. Experimental osmotic equations of state of magnetite colloids," J. Phys.: Condens. Matter **24**, 245104 (2012).
[21] E. Dubois, R. Perzynski, F. Bou, and V. Cabuil, "Liquid-gas transitions in charged colloidal dispersions: a small-angle neutron scattering coupled with phase diagrams of magnetic fluids," Langmuir **16**, 5617–5625 (2000).
[22] L. Pop and S. Odenbach, "Investigation of the microscopic reason for the magnetoviscous effect in ferrofluids studied by small angle neutron scatting," J. Phys.: Condens. Matter **18**, S2785 (2006).
[23] M. Klokkenburg, B. H. Erné, A. Wiedenmann, A. V. Petukhov, and A. P. Philipse, "Dipolar structures in magnetite ferrofluids studied with small-angle neutron scattering with and without applied magnetic field," Phys. Rev. E **75**, 051408 (2007).
[24] D. Bica, L. Vekas, M. Avdeev, O. Marinica, V. Socoliuc, M. Balasoiu, and V. Garamus, "Sterically stabilized water based magnetic fluids: Synthesis, structure and properties," J. Magn. Magn. Mater **311**, 17 (2007).
[25] A. Wiedenmann, U. Keiderling, M. Meissner, D. Wallacher, R. Gahler, R. May, S. Prevost, M. Klokkenburg, B. Erné, and J. Kohlbrecher, "Low-temperature dynamics of magnetic colloids studied by time-resolved small-angle neutron scattering," Phys. Rev. B **77**, 184417 (2008).
[26] M. V. Avdeev, E. Dubois, G. Mériguet, E. Wandersman, V. M. Garamus, A. V. Feoktystov, and R. Perzynski, "Small-angle neutron scattering analysis of a water-based magnetic fluid with charge stabilization: contrast variation and scattering of polarized neutrons," J. Appl. Crystallogr. **42**, 1009–1019 (2009).
[27] M. Barrett, A. Deschner, J. P. Embs, and M. C. Rheinstadter, "Chain formation in a magnetic fluid under the influence of strong external magnetic fields studied by small angle neutron scattering," Soft Matter **7**, 6678–6683 (2011).
[28] R. Balescu, *Equilibrium and Nonequilibrium Statistical Mechanics* (John Wiley, New York, 1975).
[29] G. N. Patey, D. Levesque, and J. J. Weis, "On the theory and computer simulations of dipolar fluids," Mol. Phys. **38**, 219 (1979).
[30] M. A. Osipov, P. I. C. Teixeira, and M. M. Telo da Gama, "Structure of strongly dipolar fluids at low densities," Phys. Rev. E **54**, 2597 (1996).
[31] J. J. Weis and D. Levesque, "Chain formation in low density dipolar hard spheres: a Monte Carlo study," Phys. Rev. Lett. **71**, 2729–2732 (1993).
[32] P. J. Camp and G. N. Patey, "Structure and scattering in colloidal ferrofluids," Phys. Rev. E **62**, 5403–5408 (2000).
[33] Z. Wang and C. Holm, "Structure and magnetization properties of polydispersed ferrofluids: A molecular dynamics study," Phys. Rev. E **68**, 041401 (2003).
[34] T. Kristóf and I. Szalai, "Magnetic properties and structure of polydisperse ferrofluid models," Phys. Rev. E **68**, 041109 (2003).
[35] P. D. Duncan and P. J. Camp, "Structure and dynamics in a monolayer of dipolar spheres," J. Chem. Phys. **121**, 11322–11331 (2004).
[36] P. Ilg, E. Coquelle, and S. Hess, "Structure and rheology of ferrofluids: simulation results and kinetic models," J. Phys.: Condens. Matter **18**, S2757 (2006).
[37] L. Luo and S. H. L. Klapp, "Fluctuations in a ferrofluid monolayer: An integral equation study," J. Chem. Phys. **131**, 034709 (2009).
[38] H. Schmidle and S. H. L. Klapp, "Phase transitions of two-dimensional dipolar fluids in external fields," J. Chem. Phys. **134**, 114903 (2011).
[39] J. Richardi and J.-J. Weis, "Low density mesostructures of confined dipolar particles in an external field," J. Chem. Phys. **135**, 124502 (2011).
[40] L. Rovigatti, J. Russo, and F. Sciortino, "No evidence of gas-liquid coexistence in dipolar hard spheres," Phys. Rev. Lett. **107**, 237801 (2011).

[41]L. Rovigatti, J. Russo, and F. Sciortino, "Structural properties of the dipolar hard-sphere fluid at low temperatures and densities," Soft Matter **8**, 6310–6319 (2012).
[42]J. Richardi and J.-J. Weis, "Influence of short range potential on field induced chain aggregation in low density dipolar particles," J. Chem. Phys. **138**, 244704 (2013).
[43]S. Kantorovich, A. O. Ivanov, L. Rovigatti, J. M. Tavares, and F. Sciortino, "Nonmonotonic magnetic susceptibility of dipolar hard-spheres at low temperature and density," Phys. Rev. Lett. **110**, 148306 (2013).
[44]E. Pyanzina, S. Kantorovich, J. J. Cerda, A. Ivanov, and C. Holm, "How to analyse the structure factor in ferrofluids with strong magnetic interactions: a combined analytic and simulation approach," Mol. Phys. **107**, 571–590 (2009).
[45]S. Kantorovich, E. Pyanzina, C. De Michele, and F. Sciortino, "How to calculate structure factors of self-assembling anisotropic particles," Soft Matter **9**, 4412–4427 (2013).
[46]E. Elfimova and A. Ivanov, "Pair correlations in magnetic nanodisperse fluids," J. Exp. Theor. Phys. **138**, 162–174 (2010).
[47]J. Cerda, E. Elfimova, V. Ballenegger, E. Krutikova, A. Ivanov, and C. Holm, "Behavior of bulky ferrofluids in the diluted low-coupling regime: Theory and simulation," Phys. Rev. E **81**, 011501 (2010).
[48]E. A. Elfimova, A. O. Ivanov, and P. J. Camp, "Theory and simulation of anisotropic pair correlations in ferrofluids in magnetic fields," J. Chem. Phys. **136**, 194502 (2012).
[49]E. Minina and S. Kantorovich, "The influence of dimensionality on the behavior of magnetic dipolar soft spheres: calculation of the pressure," J. Phys.: Condens. Matter **25**, 155102 (2013).
[50]A. O. Ivanov and S. S. Kantorovich, "Chain aggregate structure and magnetic birefringence in polydisperse ferrofluids," Phys. Rev. E **70**, 021401 (2004).
[51]L. Blum and G. Stell, "Polydisperse systems. I. Scattering function for polydisperse fluids of hard or permeable spheres," J. Chem. Phys. **71**, 42–46 (1979).
[52]P. N. Pusey, H. M. Fijnaut, and A. Vrij, "Mode amplitudes in dynamic light scattering by concentrated liquid suspensions of polydisperse hard spheres," J. Chem. Phys. **77**, 4270–4281 (1982).
[53]D. Frenkel, R. J. Vos, C. G. de Kruif, and A. Vrij, "Structure factors of polydisperse systems of hard spheres: A comparison of Monte Carlo simulations and Percus–Yevick theory," J. Chem. Phys. **84**, 4625–4630 (1986).
[54]D. A. Kofke and P. G. Bolhuis, "Freezing of polydisperse hard spheres," Phys. Rev. E **59**, 618–622 (1999).
[55]M. Hermes and M. Dijkstra, "Jamming of polydisperse hard spheres: The effect of kinetic arrest," Europhys. Lett. **89**, 38005 (2010).
[56]A. O. Ivanov and E. V. Novak, "Phase separation of ferrocolloids: The role of van der Waals interaction," Colloid J. **69**, 302–311 (2007).
[57]J. D. Weeks, D. Chandler, and H. C. Andersen, "Role of repulsive forces in determining the equilibrium structure of simple liquids," J. Chem. Phys. **54**, 5237 (1971).
[58]H. J. Limbach, A. Arnold, B. A. Mann, and C. Holm, "ESPResSo—an extensible simulation package for research on soft matter systems," Comput. Phys. Commun. **174**, 704–727 (2006).
[59]J. J. Cerdà, V. Ballenegger, O. Lenz, and C. Holm, "P3m algorithm for dipolar interactions," J. Chem. Phys. **129**, 234104 (2008).
[60]A. O. Ivanov, "Phase separation in bidisperse ferrocolloids," J. Magn. Magn. Mater. **154**, 66–70 (1996).
[61]A. Ivanov, S. Kantorovich, E. Reznikov, C. Holm, A. Pshenichnikov, A. Lebedev, A. Chremos, and P. Camp, "Magnetic properties of polydisperse ferrofluids: A critical comparison between experiment, theory and computer simulation," Phys. Rev. E **75**, 061405 (2007).
[62]J. P. Hansen and I. R. McDonald, *Theory of Simple Liquids* (Academic Press, London, 1986).
[63]S. B. Yuste and A. Santos, "Radial distribution function for hard spheres," Phys. Rev. A **43**, 5418–5423 (1991).
[64]S. B. Yuste and A. Santos, "A heuristic radial distribution function for hard disks," J. Chem. Phys. **99**, 2020–2023 (1993).